Non-reciprocal wave propagation in discretely modulated spatiotemporal plates

E. Riva, M. Di Ronco, A. Elabd, G. Cazzulani, F. Braghin

This is a post-peer-review, pre-copyedit version of an article published in Journal of Sound and Vibration. The final authenticated version is available online at:
http://dx.doi.org/10.1016/j.jsv.2020.115186

DIPARTIMENTO DI MECCANICA ■ POLITECNICO DI MILANO
via G. La Masa, 1 ■ 20156 Milano ■ EMAIL (PEC): pecmecc@cert.polimi.it
http://www.mecc.polimi.it
Rev. 0

Non-reciprocal wave propagation in discretely modulated spatiotemporal plates

E. Riva*, M. Di Ronco, A. Elabd, G. Cazzulani, F. Braghin

Politecnico di Milano
Department of Mechanical Engineering
Via La Masa 1, 20156, Milano

Abstract

We investigate non-reciprocal wave propagation in spatiotemporal phononic plates. Specifically, the first aim of this manuscript is to propose a general formulation of the Plane Wave Expansion Method (PWEM) that, in contrast with previous works, is applicable to any class of 2D spatiotemporal unit cells whose properties can be expanded in traveling plane waves. The second aim is to exploit this analysis tool in order to study a class of phononic materials capable of violating mirror symmetry in reciprocal space, therefore breaking reciprocity principle along different propagation directions in physical space. This is obtained by considering the plate elastic properties to be discretely modulated in space and continuously in time. Theoretical dispersion profiles are validated and compared with numerical simulations.

Keywords: Acoustic diode; Plane Wave Expansion Method (PWEM); non-reciprocity; phononic bandgap; space-time modulation.

1. Introduction

Non-reciprocal wave propagation in phononic crystals has drawn growing attention within the research community in the past years [1, 2]. Indeed, the opportunity to design elastic structures which support one-way wave propagation is of technological relevance for next-generation applications involving elastic energy manipulation, waveguiding and conversion [3, 4].
In this context, 1D phononic waveguides have recently been designed and

*Corresponding author. Email address: emanuele.riva@polimi.it.

successfully realized [5–8] to break the reciprocity principle. One possibility is to locally alter the material properties mimicking the propagation of a wave in mechanics [6, 9–15] and acoustics [16, 17]. This generally requires active elements such as time-modulated resonators [6] or smart periodic devices [18] driven by phase shifted modulation signals. A second possibility employs 2D lattice structures with spinning gyroscopes, establishing elastic analogues of the Quantum Hall Effect (QHE) [19–21]. This strategy relies on the exploitation of one-way topologically protected edge waves, not involving the bulk of the material. Systems with broken time reversal symmetry can be also designed using three port devices [22] or exploiting nonlinearities [23–25].

In this work we employ bi-dimensional space-time modulated systems as a platform to study non-reciprocity in mechanics. In comparison with 1D structures, the addition of one spatial dimension makes wave propagation analysis more complex, but also opens new promising ways to manipulate elastic waves along different directions. A notable example has been explored by Attarzadeh et al. [26] leveraging spatiotemporally modulated membranes to break time reversal symmetry, continuously biasing the applied traction field and material density in space and time. Although the aforementioned configuration offers a theoretical framework to study non-reciprocity in a specific class of 2D spatiotemporal mechanical structures, additional efforts are required for the analysis of arbitrarily shaped modulations. In particular, in this manuscript we aim to bridge the gap between fully continuous modulations (for which material properties are pointwise varying in time) and those unit cell profiles that can be more easily realized in engineering applications - which must be studied with appropriate tools.

For this reason, we investigate discretely modulated plates as a relevant and complete case-study. This class of materials is characterized by a spatially discrete and temporally continuous elasticity profiles which embodies non-reciprocal capabilities, achieved by inducing traveling-like material properties. In contrast with different space-time varying systems shown in previous works, this configuration allows for a more feasible implementation, which can be provided using established techniques, such as negative capacitance shunts applied to piezoelectric materials bonded on a 2D substrate [18, 27, 28]. The corresponding non-symmetric band diagram in reciprocal space is computed using a generalization of the Plane Wave Expansion Method (PWEM) extending prior works [11, 18] to 2D structures. The generalized PWEM can be applied to any kind of 2D spatiotemporal unit cells - and

not limited to any specific class of unit cell profiles - therefore assuming that the modulation can be mapped as a series of plane waves characterized by different propagation speed. Moreover, we demonstrate that discretely modulated plates support non-reciprocal wave propagation. Specifically, this is accomplished highlighting the leading Bloch-wave component [10, 11, 24, 29] of the dispersion diagram, which is characterized by a wide set of supported modes. Once the diagram is filtered to the most relevant terms, associated directivity plots and group velocities are computed to predict directional and non-reciprocal wave propagation phenomena in the $x-y$ plane. Theoretical dispersion plots are verified through numerical simulation of wave propagation and corresponding dispersion diagram, which are reconstructed from the displacement response of a plate under tone burst excitation.
The article is organized as follows: in section 2 we describe the analytical procedure for the band diagram computation of arbitrary modulations. In section 3, the PWEM is applied to a spatially discrete and temporally continuous material. Theoretical and numerical results are compared and discussed in detail. Concluding remarks are presented in section 4.

2. Analytical procedure for non-symmetric band diagram computation

Consider the general elastodynamic equation describing the out-of-plane motion of a Kirchhoff plate, therefore neglecting in-plane polarizations:

$$\frac{\partial^2 m_x}{\partial x^2} + 2\frac{\partial^2 m_{xy}}{\partial x \partial y} + \frac{\partial^2 m_y}{\partial y^2} = -\frac{\partial}{\partial t}\left[s(x,y)\rho(x,y,t)\frac{\partial w(x,y,t)}{\partial t}\right] \tag{1}$$

where $w(x,y,t)$ is the out-of-plane displacement field, $s(x,y)$ and $\rho(x,y,t)$ are the plate thickness and material density functions respectively. $m_{i,j}$ are the bending moment stress resultants, which read:

$$\begin{aligned} m_x &= B(x,y,t)\left[\frac{\partial^2 w(x,y,t)}{\partial x^2} + \nu\frac{\partial^2 w(x,y,t)}{\partial y^2}\right] \\ m_y &= B(x,y,t)\left[\frac{\partial^2 w(x,y,t)}{\partial y^2} + \nu\frac{\partial^2 w(x,y,t)}{\partial x^2}\right] \\ m_{xy} &= (1-\nu)B(x,y,t)\frac{\partial^2 w(x,y,t)}{\partial x \partial y} \end{aligned} \tag{2}$$

where $E(x,y,t)$ is the Young's Modulus and $B(x,y,t) = \frac{E(x,y,t)}{1-\nu^2}\frac{s^3(x,y)}{12}$ is the bending stiffness, which is a generic function of space and time. ν is the Poisson's ratio. Merging Eqs. 1 and 2 gives the PDE governing elastic wave propagation in modulated plates, reported in Appendix A for the sake of brevity. Now, under the assumption of space-time periodic elasticity and material density, $B(x,y,t)$ and $G(x,y,t) = s(x,y)\rho(x,y,t)$ are written in terms of exponential functions:

$$\begin{aligned} B(x,y,t) &= \sum_{h,n,v=-\infty}^{\infty} \hat{B}_{h,n,v} \mathrm{e}^{\mathrm{j}(\boldsymbol{\kappa_m}\cdot\boldsymbol{r} - v\omega_m t)} \\ G(x,y,t) &= \sum_{h,n,v=-\infty}^{\infty} \hat{G}_{h,n,v} \mathrm{e}^{\mathrm{j}(\boldsymbol{\kappa_m}\cdot\boldsymbol{r} - v\omega_m t)} \end{aligned} \tag{3}$$

where the term $\sum_{h,n,v=-\infty}^{\infty}$ denotes a nested summation over the indexes h, n, v. $\boldsymbol{\kappa_m} = (h\kappa_{mx}, n\kappa_{my})$ and $\boldsymbol{r} = (x,y)$ are the modulation wavevector and spatial coordinates mapped within the unit cell domain. We define $\kappa_{mx} = \frac{2\pi}{\lambda_{mx}}$, $\kappa_{my} = \frac{2\pi}{\lambda_{my}}$ and $\omega_m = \frac{2\pi}{T_m}$ as spatial and temporal modulation wavenumbers and frequency, with associated wavelengths λ_{mx} and λ_{my} and temporal period T_m, where the subscript $m\xi$ stands for modulation along the direction ξ. Corresponding Fourier coefficients $\hat{B}_{h,n,v}$ and $\hat{G}_{h,n,v}$ for $B(x,y,t)$ and $G(x,y,t)$ are obtained by numerical integration within the spatiotemporal domain $D = \left[-\frac{\lambda_{mx}}{2}, \frac{\lambda_{mx}}{2}\right] \times \left[-\frac{\lambda_{my}}{2}, \frac{\lambda_{my}}{2}\right] \times \left[-\frac{T_m}{2}, \frac{T_m}{2}\right]$:

$$\begin{aligned} \hat{B}_{h,n,v} &= \frac{1}{T_m \lambda_{mx} \lambda_{my}} \int_D B(x,y,t) \mathrm{e}^{-\mathrm{j}(\boldsymbol{\kappa_m}\cdot\boldsymbol{r} - v\omega_m t)} \mathrm{dD} \\ \hat{G}_{h,n,v} &= \frac{1}{T_m \lambda_{mx} \lambda_{my}} \int_D G(x,y,t) \mathrm{e}^{-\mathrm{j}(\boldsymbol{\kappa_m}\cdot\boldsymbol{r} - v\omega_m t)} \mathrm{dD} \end{aligned} \tag{4}$$

Given the 3D Fourier transform of the unit cell, a general formulation of the PWEM is hereafter presented to compute the wave propagation properties of an arbitrary profile defined within the domain D. Compared with previous studies [9, 26], this additional complexity is required in order to address more realistic case-studies, like space-time discretely modulated structures, thus not limiting the analysis to a specific set of plane waves used to describe material properties. Ansatz solution $w(x,y,t)$ is sought for Eq. 1 as combination of propagating plane waves owning the same arbitrary periodicity of

the modulation:

$$w(x,y,t) = \hat{w}(x,y,t)\mathrm{e}^{\mathrm{j}(\boldsymbol{\kappa}\cdot\boldsymbol{r}-\omega t)}, \quad \hat{w}(x,y,t) = \sum_{p,q,r=-\infty}^{\infty} \hat{W}_{p,q,r}\mathrm{e}^{\mathrm{j}(\boldsymbol{\kappa_m}\cdot\boldsymbol{r}-r\omega_m t)} \quad (5)$$

where $\boldsymbol{\kappa} = (\kappa_x, \kappa_y)$ is the imposed wavevector field and $\boldsymbol{\kappa_m} = (p\kappa_{mx}, q\kappa_{my})$. Upon combination of Eqs. 1-5 and enforcing orthogonality of exponential functions, the dispersion relation $\omega = \omega(\kappa_x, \kappa_y)$ yields:

$$\left[\tilde{\boldsymbol{L}}_0(k_x,k_y) + \tilde{\boldsymbol{L}}_1\omega + \tilde{\boldsymbol{L}}_2\omega^2\right]\tilde{\boldsymbol{w}} = 0 \quad (6)$$

which is a Quadratic Eigenvalue Problem (QEP) solved for ω imposing κ_x and κ_y. $\tilde{\boldsymbol{L}}_0(k_x,k_y)$, $\tilde{\boldsymbol{L}}_1$ and $\tilde{\boldsymbol{L}}_2$ are full matrices of dimension $\Gamma_o = (2P+1)(2Q+1)(2R+1)$, being P, Q, R the Fourier expansion truncation orders. In the remainder of the paper, the computed dispersion relations are displayed in terms of dimensionless quantities, i.e. $\mu_x = \kappa_x\lambda_{mx}$, $\mu_y = \kappa_y\lambda_{my}$, $\Omega = \omega/\omega_0$ being $\omega_0 = \kappa_m^2\sqrt{B_0/G_0}$ with $\kappa_m = \kappa_{mx}\kappa_{my}/\sqrt{\kappa_{mx}^2+\kappa_{my}^2}$, $B_0 = \frac{E_0 s_0^3}{12(1-\nu^2)}$ and $G_0 = \rho_0 s_0$. E_0, s_0, and ρ_0 are mean unit cell parameters. Moreover, a complete description of the analytical procedure and QEP matrices is provided in Appendix A.

3. Wave propagation in discretely modulated plates

Consider a periodic plate whose elasticity can be arbitrarily modulated in space and time. Specifically, in this manuscript we focus our attention on spatially discrete and temporally continuous profiles, as an relevant case-study from the engineering perspective. We assume the following function for the Young's modulus:

$$E(x,y,t) = E_0\left\{1 + \frac{\alpha_m}{2}\cos\left(\theta(x) - \omega_m t\right) + \frac{\alpha_m}{2}\cos\left(\theta(y) - \omega_m t\right)\right\}$$

$$where: \qquad \theta(\xi) = \theta(\xi + 2k\pi) \begin{cases} 0 & 0 < \xi < \frac{1}{R_s}\lambda_m \\ \dots & \dots \\ 2\pi(i-1)/R_s & \frac{i-1}{R_s}\lambda_m < \xi < \frac{i}{R_s}\lambda_m \\ \dots & \dots \\ 2\pi(R_s-1)/R_s & \frac{R_s-1}{R_s}\lambda_m < \xi < \lambda_m \end{cases}$$

$$k\ integer,\ i = 1, \dots, R_s \quad (7)$$

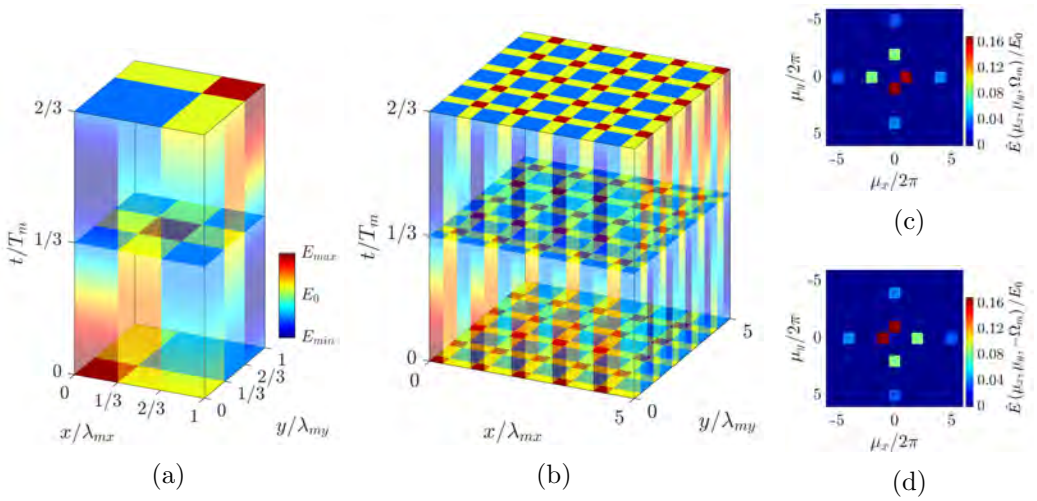

Figure 1: (a) Unit cell Young's Modulus profile in space and time. Shaded volumes represent the temporal evolution of each spatially discrete sub-element. Three different time instants are highlighted with solid surfaces for $t/T_m = 0$, $t/T_m = 1/3$ and $t/T_m = 2/3$. (b) Illustration of a finite spatio-temporal domain made of 5×5 unit cells. (c) Harmonic content of the modulation for $\Omega = \Omega_m$ (top) and $\Omega = -\Omega_m$ (bottom).

where $\alpha_m = \Delta E/E_0$ is the dimensionless modulation amplitude, $\Delta E = E_{max} - E_0$ and $E_0 = (E_{max} + E_{min})/2$ is the mean Young's Modulus value. R_s is the number of sub-elements used to discretize the unit cell spatial domain. Notice that, for simplicity and without any loss of generality, the same R_s value and lattice constant λ_m are assumed in x and y, thus $\lambda_m = \lambda_{mx} = \lambda_{my}$. Moreover, piecewise functions of space $\theta(x), \theta(y)$ define a phase shift between consecutive elements of the k^{th} unit cell, whereby their continuous modulation in time induces directional stiffness propagation, mimicking the propagation of a plane wave in a plate. This concept is elucidated in Fig. 1(a)-(b) showing that for $R_s = 3$ the elastic properties are tailored to propagate along an angle of $\pi/4$ in the $x-y$ plane. Interestingly, the spatial discretization generates a set of traveling plane wave components that, in general, populate the entire $\mu_x \times \mu_y \times \Omega$ reciprocal domain, whereby their propagation velocity (positive or negative) defines the non-reciprocal working direction of the gaps [9, 11]. That is, the spectral content resulting from the unit cell 3DFT, which has nonzero components only in the $\mu_x \times \mu_y \times \Omega_m$ subspace (see Fig. 1(c)-(d)), reveals counter propagating harmonics at different spatial wavenumbers and same frequency Ω_m. These components have

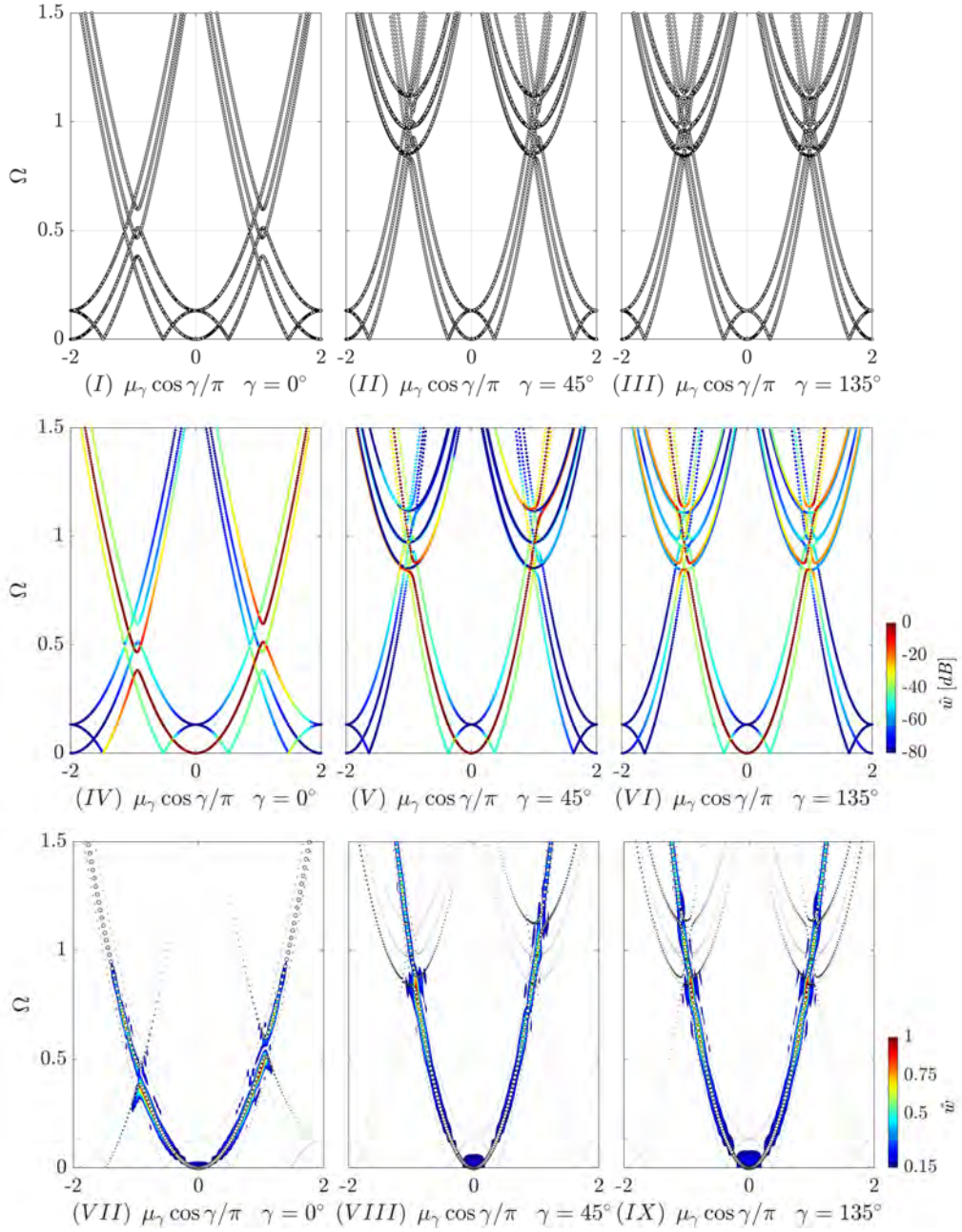

Figure 2: $(I) - (III)$ Dispersion relation $\Omega = \Omega(\mu_x, \mu_y)$ for $\gamma = 0$, $\gamma = \pi/4$ and $\gamma = 3/4\pi$. $(IV) - (VI)$ Colored dispersion relation $\Omega = \Omega(\mu_x, \mu_y)$ as a function of the magnitude of the associated eigenvector component $|w|$ [dB]. $(VII) - (IX)$ Comparison between numerical simulations and leading dispersion branches.

different propagation speed in physical space which, in turn, depends upon modulation wavenumbers and frequency: i.e. $\boldsymbol{v_m} = \omega_m / (h\kappa_{mx}, n\kappa_{mx})$ for different h, n values, and they all contribute to the unit cell displayed in Fig. 1(a). For simplicity, in the remainder of the manuscript we consider a dimensionless modulation velocity vector $\boldsymbol{\beta_m} = (\beta_{mx}, \beta_{my})$ relative to the first plane wave component, i.e. for $h = 1$ and $n = 1$:

$$\beta_{m\xi} = \frac{\omega_m}{\kappa_{m\xi}} \frac{1}{\kappa_m \sqrt{\frac{B_0}{G_0}}} = \frac{v_{m\xi}}{\kappa_m \sqrt{\frac{B_0}{G_0}}} \tag{8}$$

and $\gamma_m = \arctan(\beta_{my}/\beta_{mx})$ defines its propagation direction. Plugging the aforementioned 3D Fourier expansion of $E(x, y, t)$ for $\beta_{mx} = \beta_{my} = \beta_m = 0.094$, $\alpha_m = 0.8$ (such strong modulation is needed in order to generate a sufficient amplitude associated with the first nonzero spectral component of the unit cell, as shown in Fig. 1(c)-(d)) and $\lambda_{mx} = \lambda_{my} = \lambda_m = 0.06\ m$ into Eq. 6 and considering constant material density $G(x, y, t) = G$, gives the associated dispersion relation, which is represented in Fig. 2 $(I) - (III)$ mapped along different wave propagation directions, i.e. $\gamma = 0,\ \pi/4$ and $3/4\pi$ respectively, where $\mu_\gamma = \sqrt{\mu_x^2 + \mu_y^2}$ defines the dimensionless propagation constant, being $\gamma = \arctan(\mu_y/\mu_x)$ the investigation direction. It is worth mentioning that, given the unit cell spatial discretization, the associated spectral content shown in Fig. 1(c) is richer compared to point-to-point modulations. As a result, the Bloch diagram increases in complexity and the number of dispersion branches is consistent with the harmonics used to approximate the wave solution. In the case at hand, $P = 3, Q = 3, R = 1$ are employed, whereby the series expansion is limited to $(2P + 1)(2Q + 1)$ spatial and $(2R + 1)$ temporal harmonics. These additional modes populate the entire frequency-wavenumber space, which is in agreement with the behavior of 1D space-time modulated systems [11, 15, 24, 29]. To discriminate the most relevant dispersion branches, each eigenvalue is weighted by the magnitude of the associated eigenvector component. That is, consider the wave solution for $\omega = \hat{\omega}$ and $\boldsymbol{\kappa} = \hat{\boldsymbol{\kappa}}$:

$$w(x, y, t) = \sum_{p,q,r=-P,-Q,-R}^{P,Q,R} \hat{W}_{p,q,r} \mathrm{e}^{\mathrm{j}(\boldsymbol{\kappa_m} \cdot \boldsymbol{r} - r\omega_m t)} \mathrm{e}^{\mathrm{j}(\hat{\boldsymbol{\kappa}} \cdot \boldsymbol{r} - \hat{\omega} t)} \tag{9}$$

since the QEP is ω_m-periodic and $\boldsymbol{\kappa_m}$-periodic, the solution at a given frequency and wavenumber is equivalent to that computed at $\omega = \hat{\omega} + r\omega_m$ and

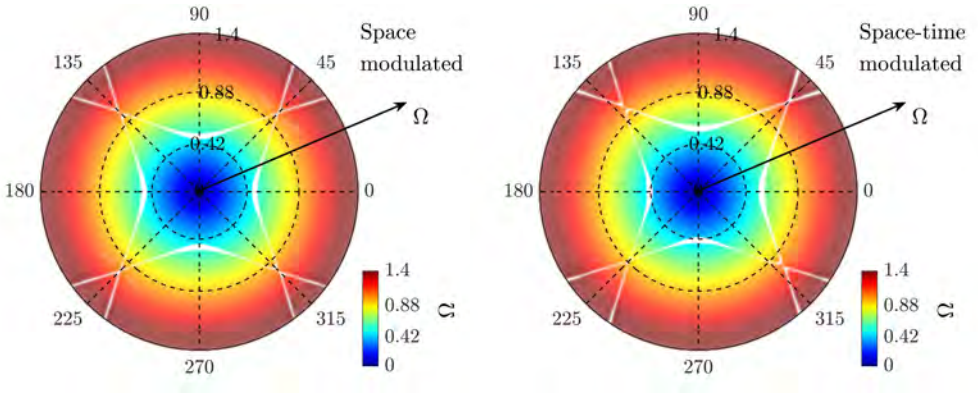

(a) (b)

Figure 3: Directivity plots for (a) spatially modulated plate $\alpha_m = 0.8$, $\beta_m = 0$ and (b) spatiotemporal modulation $\alpha_m = 0.8$, $\beta_m = 0.094$.

$\boldsymbol{\kappa} = \hat{\boldsymbol{\kappa}} + (p\kappa_{mx}, q\kappa_{my})$ and the eigenvector components $\hat{W}_{p,q,r}$ are shifted in position accordingly. For this reason, one can identify the amplitude associated with the contribution of the p, q, r branch to that of the $p = 0, q = 0, r = 0$ component while probing the entire family of solutions given by the QEP in Eq. 6. The resulting dispersion, obtained assigning a color proportional to the amplitude $|\hat{W}_{0,0,0}(\omega, \boldsymbol{\kappa})|$, is illustrated in Fig. 2 $(IV) - (VI)$, which reveals that the energy content is mostly located on the central branches, whereby highlighting that opposite wavenumbers support gaps occurring at different frequencies. Specifically, at $\Omega^+ = 0.55$ and $\Omega^- = 0.42$ for $\gamma = 0$ (see Fig. 2 $((III))$), where the superscripts $+$ and $-$ denote bandgap central frequencies for positive and negative wavenumbers, respectively. Higher relative distance between $\Omega^+ = 1.1$ and $\Omega^- = 0.88$ is achieved for $\gamma = \pi/4$ (Fig. $((IV))$), whereas reciprocal bandgaps are obtained for $\Omega = 0.88$ and $\Omega = 1.1$ along $\gamma = 3/4\pi$.

In the remainder of this section we restrict the wave propagation analysis to the leading components, i.e. the red highlighted eigensolutions which are characterized by $|\hat{W}_{0,0,0}(\omega, \boldsymbol{\kappa})| = 1$, thus neglecting higher order harmonics, as wave propagation occurs involving mainly the terms associated with the central branch. This approximation is verified though numerical simulations of wave propagation performed using the commercial software COMSOL Multiphysics. Specifically,we consider a plate made of 90×90 unit cells which is forced in its central region using a wide spectrum tone

burst excitation. The displacement field is integrated within the spatial and temporal simulation domains to obtain the numerical Bloch diagram, proving good agreement with the analytical results, as shown in the comparison in Figs. 2 $(VII) - (IX)$ for $\gamma = 0,\ \pi/4$, and $3/4\pi$ respectively.
A more complete description of the filtered eigensolution for spatial and spatiotemporal modulations is presented in Figs. 3(a)-3(b), in terms of directivity plot: $\Omega(\mu_x, \mu_y)$ is mapped in a polar plane, where Ω is the distance from the origin (also represented with colors) and $\gamma = \arctan(\mu_y/\mu_x)$ is the corresponding angle. When the spatial modulation is turned on, a Bragg-bandgap opens, and its position in the frequency domain depends upon the direction of interest γ. The addition of a temporal periodicity results into a modulation-induced tilting of the frequency-wavenumber space, which is illustrated in the asymmetric plot in Fig. 3(b) and reflects the presence of directional plane wave components in the unit cell 3DFT in Fig. 1(c)-(d). The amount of change in the bandgap central position is dependent upon γ (as for purely spatially modulated plate) but also from the modulation direction of propagation γ_m: indeed, for $\gamma = \gamma_m = \pi/4$ the dispersion relation is more asymmetric, i.e. Ω^+ and Ω^- move toward higher and lower frequencies respectively, while the bias decreases until it nullifies for $\gamma = \frac{3}{4}\pi \pm \pi$, a direction along which mirror symmetry is preserved and $\Omega^+ = \Omega^- = \Omega$, similarly to spatiotemporal membranes [26].
Consider now the non-reciprocal wave propagation problem between two points A (emitter) and B (receiver). Point A is located in the central region of the plate, whereas B is set sufficiently far from the excitation. When the system is forced waves propagate along the direction identified by the group velocity field $C_g = \nabla\Omega(\mu_x, \mu_y)$, which is illustrated in Figs. 4(a)-4(b) for spatially and spatiotemporally modulated medium. It is worth mentioning that C_g is computed considering the filtered dispersion in Fig. 3, therefore assuming that wave propagation occurs not involving less relevant, higher order solutions that would have led to additional group velocity components at every frequency associated with negligible wave amplitude.
Thanks to space-time modulation, C_g is defined only for certain angular regions, as the filtered dispersion $\Omega(\mu_x, \mu_y)$ embodies non mirror-symmetric properties. A non-reciprocal device can be thus achieved when the receiver B is located within $[160°, 200°]$ and $[250°, 290°]$ for $\Omega \approx 0.42$, as opposite directions (i.e. for $[-20°, 20°]$ and $[70°, 110°]$) support wave propagation. Non-reciprocity is confirmed by the RMS of the displacement field in Fig. 4(d) obtained by numerical simulation under narrowband spectrum excita-

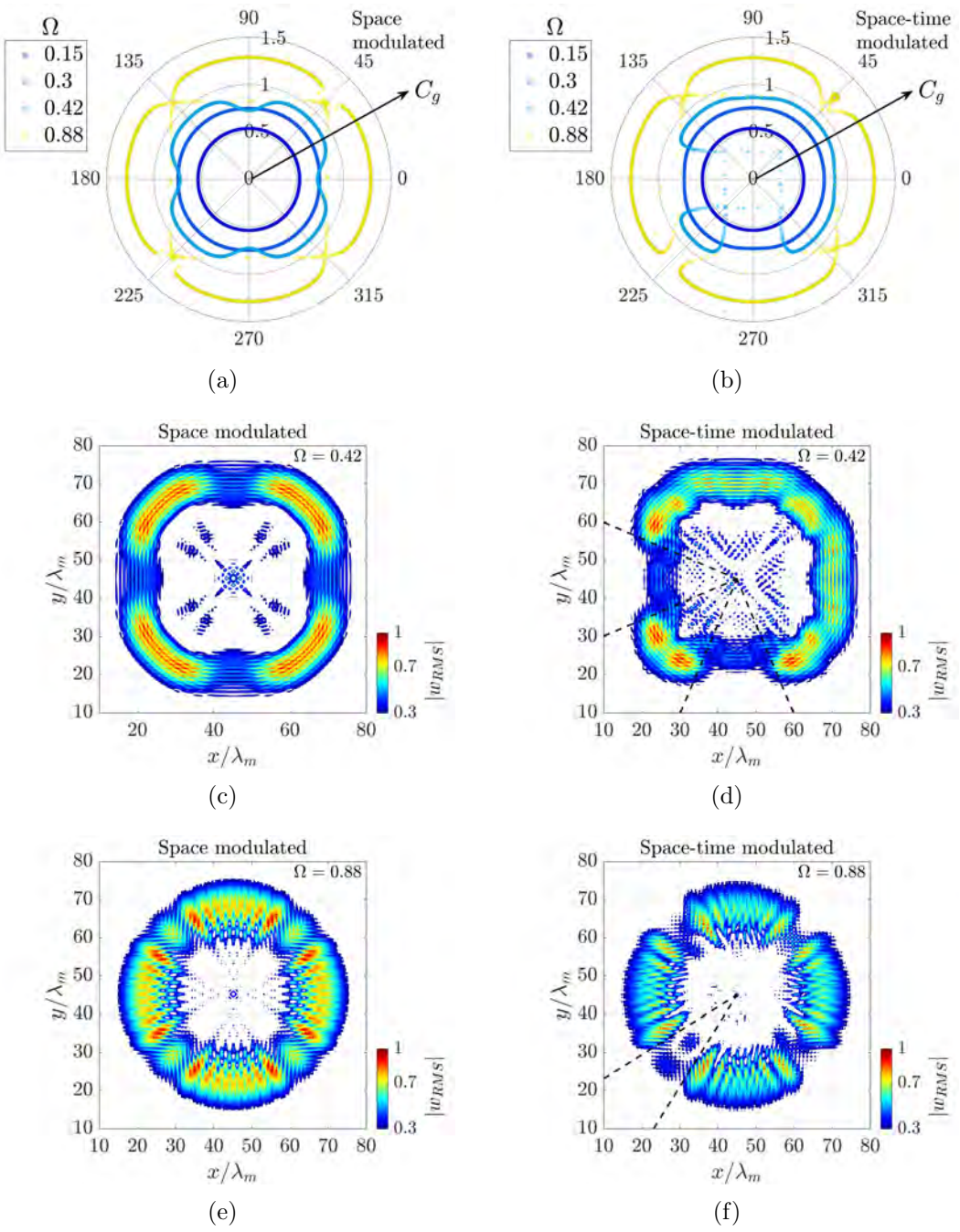

Figure 4: (a)-(b) Group velocity fields at different frequency levels. RMS of the displacement field for spatially and spatiotemporally modulated plate under narrowband tone burst excitation centered at (c)-(d) $\Omega = 0.42$ and (e)-(f) $\Omega = 0.88$.

tion. To better highlight the asymmetric behavior, Fig. 4(d) illustrates the RMS response computed for the final instants of the time history. The resulting transmitted signal is clearly non-reciprocal for waves propagating along opposite directions. For ease of visualization, the agreement between group velocity and time simulations is shown by superimposing the limits of non-reciprocal regions (dashed black lines) to the RMS displacement field. This behavior can be also obtained within $[-20°, 20°]$ and $[70°, 110°]$ by switching from positive to negative modulation direction. Moreover, if the temporal modulation is turned off, the same input forcing gives the RMS displacement field in Fig. 4(c), thus preserving wave propagation mirror symmetry, consistently with the corresponding group velocity line depicted in Fig. 4(a). Fig. 4(c) also reveals the presence of reciprocal gaps close to the burst excitation central frequencies which leads to the stop regions centered at $0, 90°, 180°$ and $270°$. The comparison between Figs. 4(a)-4(c) and 4(b)-4(d) illustrates that temporal and spatial modulations can be combined, resulting in a time reversal symmetry break along specific directions, which can be analytically predicted using a general formulation of the PWEM.
Non-reciprocity is also achieved within a narrow angular region centered at $225°$ for $\Omega \approx 0.88$, i.e. along the direction of propagation of the modulation, as shown by the corresponding group velocity and RMS displacement fields in Figs. 4(b)-4(f) respectively. On the other hand, when the temporal modulation is turned off, reciprocity is restored, as shown in Fig. 4(e) for a spatially varying medium forced at $\Omega \approx 0.88$. Even though the modulation amplitude is not enough to generate a wide non-reciprocal region, the wave propagation characteristics are well captured by the group velocity field, which suggests asymmetric behavior along the angular regions highlighted with black dashed lines.

4. Conclusions

In this work we proposed a general formulation of the PWEM in order to study non-reciprocal wave propagation in spatiotemporally modulated plates. This analysis tool is applicable to any class of modulations that can be written as a series of traveling plane waves, thus extending the allowable modulation classes that can be studied with the analytical tools present in the literature.
In the second part of the manuscript, the generalized PWEM has been applied to study a spatially discrete and temporally continuous elastic medium

which embodies non-reciprocal capabilities. We computed directivity and group velocity plots, which are used to predict directional and non-reciprocal phenomena at specific frequencies. Theoretical solutions have been compared to numerical results, proving that the generalized PWEM is able to describe wave propagation properties of discretely space-time modulated systems.

Acknowledgments

Support by the Italian Ministry of Education, University and Research, through the project Department of Excellence LIS4.0 (Integrated Laboratory for Lightweight and Smart Structures), is acknowledged.

Appendix A. QEP matrices description

Consider the wave propagation problem described in Section 2. The general equation governing the out of plane dynamic for a Kirchhoff plate reads:

$$\begin{aligned} &B\left[\frac{\partial^4 w}{\partial x^4}+2\frac{\partial^4 w}{\partial x^2\partial y^2}+\frac{\partial^4 w}{\partial y^4}\right]+2\frac{\partial B}{\partial x}\frac{\partial}{\partial x}\left[\frac{\partial^2 w}{\partial x^2}+\frac{\partial^2 w}{\partial y^2}\right]+2\frac{\partial B}{\partial y}\frac{\partial}{\partial y}\left[\frac{\partial^2 w}{\partial x^2}+\frac{\partial^2 w}{\partial y^2}\right]+\\ &+\left[\frac{\partial^2 B}{\partial x^2}+\frac{\partial^2 B}{\partial y^2}\right]\left[\frac{\partial^2 w}{\partial x^2}+\frac{\partial^2 w}{\partial y^2}\right]-(1-\nu)\left[\frac{\partial^2 B}{\partial x^2}\frac{\partial^2 w}{\partial y^2}-2\frac{\partial^2 B}{\partial x\partial y}\frac{\partial^2 w}{\partial x\partial y}+\frac{\partial^2 B}{\partial y^2}\frac{\partial^2 w}{\partial x^2}\right]=\\ &=-\frac{\partial G}{\partial t}\frac{\partial w}{\partial t}-G\frac{\partial^2 w}{\partial t^2} \end{aligned} \tag{A.1}$$

Plugging Eqs. 3-5 into Eq. A.1 gives:

$$\begin{aligned} &\sum_{h,n,v,p,q,r}\hat{B}_{h,n,v}\hat{W}_{p,q,r}\Bigg\{\Big[(pk_{mx}+k_x)^2+(qk_{my}+k_y)^2\Big]\Big[([h+p]k_{mx}+k_x)^2+([n+q]k_{my}+k_y)^2\Big]+\\ &-(1-\nu)\Big[(hk_{mx})(qk_{my}+k_y)-(nk_{my})(pk_{mx}+k_x)\Big]^2\Bigg\}\cdot \mathrm{e}^{\mathrm{j}([h+p]k_{mx}x+[n+q]k_{my}y-[v+r]\omega_m t)}=\\ &=\sum_{h,n,v,p,q,r}\hat{G}_{h,n,v}\hat{W}_{p,q,r}\Big\{(r\omega_m+\omega)([v+r]\omega_m+\omega)\Big\}\cdot \mathrm{e}^{\mathrm{j}([h+p]k_{mx}x+[n+q]k_{my}y-[v+r]\omega_m t)} \end{aligned} \tag{A.2}$$

which can be simplified exploiting the orthogonality of the Fourier basis, thus all the terms are multiplied by $\mathrm{e}^{-\mathrm{j}(ak_{mx}x+bk_{my}y-c\omega_m t)}$ and integrated over $D=\left[-\frac{\lambda_{mx}}{2},\frac{\lambda_{mx}}{2}\right]\times\left[-\frac{\lambda_{my}}{2},\frac{\lambda_{my}}{2}\right]\times\left[-\frac{T_m}{2},\frac{T_m}{2}\right]$. Eq. (A.2), can now be

conveniently rewritten as:

$$\sum_{p=-P}^{P}\sum_{q=-Q}^{Q}\sum_{r=-R}^{R}\hat{B}_{a-p,b-q,c-r}\hat{W}_{p,q,r}\Big\{\Big[(pk_{mx}+k_x)^2+(qk_{my}+k_y)^2\Big]\Big[(ak_{mx}+k_x)^2+(bk_{my}+k_y)^2\Big]+$$
$$-(1-\nu)\Big[([a-p]k_{mx})(qk_{my}+k_y)-([b-q]k_{my})(pk_{mx}+k_x)\Big]^2\Big\}=$$
$$=\sum_{p=-P}^{P}\sum_{q=-Q}^{Q}\sum_{r=-R}^{R}\hat{G}_{a-p,b-q,c-r}\hat{W}_{p,q,r}\Big\{(r\omega_m+\omega)(c\omega_m+\omega)\Big\} \tag{A.3}$$

Eq. A.3 is a QEP, which can be written using a compact matrix notation, expanding the inner summation terms:

$$\sum_{p=-P}^{P}\sum_{q=-Q}^{Q}\tilde{\boldsymbol{K}}_{a-p,b-q}\Big\{\Big[(pk_{mx}+k_x)^2+(qk_{my}+k_y)^2\Big]\Big[(ak_{mx}+k_x)^2+(bk_{my}+k_y)^2\Big]+$$
$$-(1-\nu)\Big[([a-p]k_{mx})(qk_{my}+k_y)-([b-q]k_{my})(pk_{mx}+k_x)\Big]^2\Big\}\tilde{\boldsymbol{w}}_{p,q}=$$
$$=\sum_{p=-P}^{P}\sum_{q=-Q}^{Q}\Big\{\tilde{\boldsymbol{M}}^0_{a-p,b-q}+\tilde{\boldsymbol{M}}^1_{a-p,b-q}\omega+\tilde{\boldsymbol{M}}^2_{a-p,b-q}\omega^2\Big\}\tilde{\boldsymbol{w}}_{p,q} \tag{A.4}$$

where $\tilde{\boldsymbol{K}}_{a-p,b-q}$, $\tilde{\boldsymbol{M}}^0_{a-p,b-q}$, $\tilde{\boldsymbol{M}}^1_{a-p,b-q}$, $\tilde{\boldsymbol{M}}^2_{a-p,b-q}$ are full square matrices of size $(2R+1)$:

$$\tilde{\boldsymbol{K}}_{a-p,b-q}=\begin{bmatrix}\hat{B}_{a-p,b-q,0} & \dots & \hat{B}_{a-p,b-q,-2R}\\ \vdots & \ddots & \vdots\\ \hat{B}_{a-p,b-q,2R} & \dots & \hat{B}_{a-p,b-q,0}\end{bmatrix}$$

$$\tilde{\boldsymbol{M}}^0_{a-p,b-q}=\begin{bmatrix}\hat{G}_{a-p,b-q,0}(-R)(-R) & \dots & \hat{G}_{a-p,b-q,-2R}(-R)(+R)\\ \vdots & \ddots & \vdots\\ \hat{G}_{a-p,b-q,2R}(+R)(-R) & \dots & \hat{G}_{a-p,b-q,0}(+R)(+R)\end{bmatrix}\omega_m^2$$

$$\tilde{\boldsymbol{M}}^1_{a-p,b-q}=\begin{bmatrix}\hat{G}_{a-p,b-q,0}(-R-R) & \dots & \hat{G}_{a-p,b-q,-2R}(-R+R)\\ \vdots & \ddots & \vdots\\ \hat{G}_{a-p,b-q,2R}(+R-R) & \dots & \hat{G}_{a-p,b-q,0}(+R+R)\end{bmatrix}\omega_m$$

$$\tilde{\boldsymbol{M}}^2_{a-p,b-q}=\begin{bmatrix}\hat{G}_{a-p,b-q,0} & \dots & \hat{G}_{a-p,b-q,-2R}\\ \vdots & \ddots & \vdots\\ \hat{G}_{a-p,b-q,2R} & \dots & \hat{G}_{a-p,b-q,0}\end{bmatrix}$$

and $\tilde{\boldsymbol{w}}_{p,q}$ accommodates the $(2R+1)$ time-harmonic components:

$$\tilde{\boldsymbol{w}}_{p,q}=\{w_{p,q,-R},\dots,w_{p,q,+R}\}^T$$

In the same way, the summation term $q \in [-Q, Q]$ can be expanded, thus:

$$\sum_{p=-P}^{P} \left(\tilde{\boldsymbol{Z}}^0_{a-p} + \tilde{\boldsymbol{Z}}^1_{a-p}\omega + \tilde{\boldsymbol{Z}}^2_{a-p}\omega^2 \right) \tilde{\boldsymbol{w}}_p = 0 \tag{A.5}$$

where $\tilde{\boldsymbol{Z}}^0_{a-p}$, $\tilde{\boldsymbol{Z}}^1_{a-p}$, $\tilde{\boldsymbol{Z}}^2_{a-p}$ are full square matrices of order $(2Q+1)(2R+1)$ which take the following form:

$$\tilde{\boldsymbol{Z}}^0_{a-p} = \begin{bmatrix} \tilde{\boldsymbol{M}}^0_{a-p,0} + & & \tilde{\boldsymbol{M}}^0_{a-p,-2Q} + \\ -\tilde{\boldsymbol{K}}_{a-p,0}\Big\{\Big[(pk_{mx}+k_x)^2+(-Qk_{my}+k_y)^2\Big]\cdot & & -\tilde{\boldsymbol{K}}_{a-p,-2Q}\Big\{\Big[(pk_{mx}+k_x)^2+(+Qk_{my}+k_y)^2\Big]\cdot \\ \cdot\Big[(ak_{mx}+k_x)^2+(-Qk_{my}+k_y)^2\Big]+ & \cdots & \cdot\Big[(ak_{mx}+k_x)^2+(-Qk_{my}+k_y)^2\Big]+ \\ -(1-\nu)\Big[([a-p]k_{mx})(-Qk_{my}+k_y)+ & & -(1-\nu)\Big[([a-p]k_{mx})(+Qk_{my}+k_y)+ \\ -([-Q+Q]k_{my})(pk_{mx}+k_x)\Big]^2\Big\} & & -([-Q-Q]k_{my})(pk_{mx}+k_x)\Big]^2\Big\} \\ \vdots & \ddots & \vdots \\ \tilde{\boldsymbol{M}}^0_{a-p,2Q} + & & \tilde{\boldsymbol{M}}^0_{a-p,0} + \\ -\tilde{\boldsymbol{K}}_{a-p,2Q}\Big\{\Big[(pk_{mx}+k_x)^2+(-Qk_{my}+k_y)^2\Big]\cdot & & -\tilde{\boldsymbol{K}}_{a-p,0}\Big\{\Big[(pk_{mx}+k_x)^2+(+Qk_{my}+k_y)^2\Big]\cdot \\ \cdot\Big[(ak_{mx}+k_x)^2+(+Qk_{my}+k_y)^2\Big]+ & \cdots & \cdot\Big[(ak_{mx}+k_x)^2+(+Qk_{my}+k_y)^2\Big]+ \\ -(1-\nu)\Big[([a-p]k_{mx})(-Qk_{my}+k_y)+ & & -(1-\nu)\Big[([a-p]k_{mx})(+Qk_{my}+k_y)+ \\ -([+Q+Q]k_{my})(pk_{mx}+k_x)\Big]^2\Big\} & & -([+Q-Q]k_{my})(pk_{mx}+k_x)\Big]^2\Big\} \end{bmatrix}$$

$$\tilde{\boldsymbol{Z}}^1_{a-p} = \begin{bmatrix} \tilde{\boldsymbol{M}}^1_{a-p,0} & \cdots & \tilde{\boldsymbol{M}}^1_{a-p,-2Q} \\ \vdots & \ddots & \vdots \\ \tilde{\boldsymbol{M}}^1_{a-p,2Q} & \cdots & \tilde{\boldsymbol{M}}^1_{a-p,0} \end{bmatrix}$$

$$\tilde{\boldsymbol{Z}}^2_{a-p} = \begin{bmatrix} \tilde{\boldsymbol{M}}^2_{a-p,0} & \cdots & \tilde{\boldsymbol{M}}^2_{a-p,-2Q} \\ \vdots & \ddots & \vdots \\ \tilde{\boldsymbol{M}}^2_{a-p,2Q} & \cdots & \tilde{\boldsymbol{M}}^2_{a-p,0} \end{bmatrix}$$

which is further expanded for $p \in [-P, P]$ wave components:

$$\left[\tilde{\boldsymbol{L}}_0(k_x, k_y) + \tilde{\boldsymbol{L}}_1\omega + \tilde{\boldsymbol{L}}_2\omega^2 \right] \tilde{\boldsymbol{w}} = 0 \tag{A.6}$$

where $\tilde{\boldsymbol{L}}_0(k_x, k_y)$, $\tilde{\boldsymbol{L}}_1$, $\tilde{\boldsymbol{L}}_2$ are full square matrices of order $(2P+1)(2Q+1)(2R+1)$:

$$\tilde{\boldsymbol{L}}_0(k_x, k_y) = \begin{bmatrix} \tilde{\boldsymbol{Z}}_0^0 & \cdots & \tilde{\boldsymbol{Z}}_{-2P}^0 \\ \vdots & \ddots & \vdots \\ \tilde{\boldsymbol{Z}}_{2P}^0 & \cdots & \tilde{\boldsymbol{Z}}_0^0 \end{bmatrix}$$

$$\tilde{\boldsymbol{L}}_1 = \begin{bmatrix} \tilde{\boldsymbol{Z}}_0^1 & \cdots & \tilde{\boldsymbol{Z}}_{-2P}^1 \\ \vdots & \ddots & \vdots \\ \tilde{\boldsymbol{Z}}_{2P}^1 & \cdots & \tilde{\boldsymbol{Z}}_0^1 \end{bmatrix}$$

$$\tilde{\boldsymbol{L}}_2 = \begin{bmatrix} \tilde{\boldsymbol{Z}}_0^2 & \cdots & \tilde{\boldsymbol{Z}}_{-2P}^2 \\ \vdots & \ddots & \vdots \\ \tilde{\boldsymbol{Z}}_{2P}^2 & \cdots & \tilde{\boldsymbol{Z}}_0^2 \end{bmatrix}$$

References

[1] A. Maznev, A. Every, O. Wright, Reciprocity in reflection and transmission: What is a 'phonon diode'?, Wave Motion 50 (4) (2013) 776–784 (2013).

[2] M. B. Zanjani, A. R. Davoyan, A. M. Mahmoud, N. Engheta, J. R. Lukes, One-way phonon isolation in acoustic waveguides, Applied Physics Letters 104 (8) (2014) 081905 (2014).

[3] H. Nassar, H. Chen, A. Norris, M. Haberman, G. Huang, Non-reciprocal wave propagation in modulated elastic metamaterials, Proc. R. Soc. a 473 (2202) (2017) 20170188 (2017).

[4] K. Yi, M. Collet, S. Karkar, Frequency conversion induced by time-space modulated media, Physical review B 96 (10) (2017) 104110 (2017).

[5] M. Attarzadeh, J. Callanan, M. Nouh, Experimental observation of non-reciprocal waves in a resonant metamaterial beam, arXiv preprint arXiv:1910.08765 (2019).

[6] Y. Chen, X. Li, H. Nassar, A. N. Norris, C. Daraio, G. Huang, Non-reciprocal wave propagation in a continuum-based metamaterial with space-time modulated resonators, Physical Review Applied 11 (6) (2019) 064052 (2019).

[7] Y. Wang, B. Yousefzadeh, H. Chen, H. Nassar, G. Huang, C. Daraio, Observation of nonreciprocal wave propagation in a dynamic phononic lattice, Physical review letters 121 (19) (2018) 194301 (2018).

[8] Y. Chen, X. Li, H. Nassar, A. N. Norris, C. Daraio, G. Huang, Nonreciprocal wave propagation in a continuum-based metamaterial with space-time modulated resonators, Phys. Rev. Applied 11 (2019) 064052 (Jun 2019). doi:10.1103/PhysRevApplied.11.064052.
URL `https://link.aps.org/doi/10.1103/PhysRevApplied.11.064052`

[9] G. Trainiti, M. Ruzzene, Non-reciprocal elastic wave propagation in spatiotemporal periodic structures, New Journal of Physics 18 (8) (2016) 083047 (2016).

[10] J. Vila, R. K. Pal, M. Ruzzene, G. Trainiti, A bloch-based procedure for dispersion analysis of lattices with periodic time-varying properties, Journal of Sound and Vibration 406 (2017) 363–377 (2017).

[11] E. Riva, J. Marconi, G. Cazzulani, F. Braghin, Generalized plane wave expansion method for non-reciprocal discretely modulated waveguides, Journal of Sound and Vibration (2019).

[12] J. Marconi, G. Cazzulani, E. Riva, F. Braghin, Observations on the behavior of discretely modulated spatiotemporal periodic structures, in: Active and Passive Smart Structures and Integrated Systems XII, Vol. 10595, International Society for Optics and Photonics, Denver, Colorado, United States, 2018, p. 105952N (2018).

[13] M. Attarzadeh, M. Nouh, Elastic wave propagation in moving phononic crystals and correlations with stationary spatiotemporally modulated systems, AIP Advances 8 (10) (2018) 105302 (2018).

[14] M. A. Attarzadeh, S. Maleki, J. L. Crassidis, M. Nouh, Non-reciprocal wave phenomena in energy self-reliant gyric metamaterials, The Journal of the Acoustical Society of America 146 (1) (2019) 789–801 (2019). arXiv:https://doi.org/10.1121/1.5114916, doi:10.1121/1.5114916.
URL https://doi.org/10.1121/1.5114916

[15] J. Huang, X. Zhou, A time-varying mass metamaterial for non-reciprocal wave propagation, International Journal of Solids and Structures 164 (2019) 25–36 (2019).

[16] J. Li, C. Shen, X. Zhu, Y. Xie, S. A. Cummer, Nonreciprocal sound propagation in space-time modulated media, Physical Review B 99 (14) (2019) 144311 (2019).

[17] N. Geib, A. Sasmal, K. Grosh, B. I. Popa, Y. Zhai, Design and fabrication of a linear broadband non-reciprocal acoustic waveguide using feedforward control, The Journal of the Acoustical Society of America 145 (3) (2019) 1687–1687 (2019).

[18] J. Marconi, E. Riva, M. Di Ronco, G. Cazzulani, F. Braghin, M. Ruzzene, Experimental observation of non-reciprocal band-gaps in a space-time modulated beam using a shunted piezoelectric array, arXiv preprint arXiv:1909.13224 (2019).

[19] P. Wang, L. Lu, K. Bertoldi, Topological phononic crystals with one-way elastic edge waves, Physical review letters 115 (10) (2015) 104302 (2015).

[20] C. L. Kane, E. J. Mele, Quantum spin hall effect in graphene, Physical review letters 95 (22) (2005) 226801 (2005).

[21] H. Chen, L. Yao, H. Nassar, G. Huang, Mechanical quantum hall effect in time-modulated elastic materials, Physical Review Applied 11 (4) (2019) 044029 (2019).

[22] R. Fleury, D. L. Sounas, A. Alù, Subwavelength ultrasonic circulator based on spatiotemporal modulation, Physical Review B 91 (17) (2015) 174306 (2015).

[23] A. Merkel, M. Willatzen, J. Christensen, Dynamic nonreciprocity in loss-compensated piezophononic media, Physical Review Applied 9 (3) (2018) 034033 (2018).

[24] S. P. Wallen, M. R. Haberman, Nonreciprocal wave phenomena in spring-mass chains with effective stiffness modulation induced by geometric nonlinearity, Physical Review E 99 (1) (2019) 013001 (2019).

[25] M. D. Fronk, S. Tawfick, C. Daraio, S. Li, A. Vakakis, M. J. Leamy, Acoustic non-reciprocity in lattices with nonlinearity, internal hierarchy, and asymmetry: Computational study, Journal of Vibration and Acoustics 141 (5) (2019) 051011 (2019).

[26] M. Attarzadeh, M. Nouh, Non-reciprocal elastic wave propagation in 2d phononic membranes with spatiotemporally varying material properties, Journal of Sound and Vibration 422 (2018) 264–277 (2018).

[27] G. Trainiti, Y. Xia, J. Marconi, G. Cazzulani, A. Erturk, M. Ruzzene, Time-periodic stiffness modulation in elastic metamaterials for selective wave filtering: Theory and experiment, Phys. Rev. Lett. 122 (2019) 124301 (Mar 2019). doi:10.1103/PhysRevLett.122.124301.
URL https://link.aps.org/doi/10.1103/PhysRevLett.122.124301

[28] B. De Marneffe, A. Preumont, Vibration damping with negative capacitance shunts: theory and experiment, Smart Materials and Structures 17 (3) (2008) 035015 (2008).

[29] B. M. Goldsberry, S. P. Wallen, M. R. Haberman, Non-reciprocal wave propagation in mechanically-modulated continuous elastic metamaterials, The Journal of the Acoustical Society of America 146 (1) (2019) 782–788 (2019).